New Candidates for Topological Insulators : Pb-based chalcogenide series

Hosub Jin,[1] Jung-Hwan Song,[1,*] Arthur J. Freeman,[1] and Mercouri G. Kanatzidis[2]

[1]*Department of Physics and Astronomy, Northwestern University, Evanston, Illinois 60208, USA*

[2]*Department of Chemistry, Northwestern University, Evanston, Illinois 60208, USA*

Abstract

To date, Bi_2Se_3 is known as the best three-dimensional high temperature topological insulator with a large bulk band gap. Here, we theoretically predict that the series of Pb-based layered chalcogenides, $Pb_nBi_2Se_{n+3}$ and $Pb_nSb_2Te_{n+3}$, are possible new candidates for topological insulators. As n increases, the phase transition from a topological insulator to a band insulator is found to occur between $n = 2$ and 3 for both series. Significantly, among the new topological insulators, we found a bulk band gap of 0.40eV in $PbBi_2Se_4$ which is one of the largest gap topological insulators, and that $Pb_2Sb_2Te_5$ is located in the immediate vicinity of the topological phase boundary, making its topological phase easily tunable by changing external parameters such as lattice constants. Due to the three-dimensional Dirac cone at the phase boundary, massless Dirac fermions also may be easily accessible in $Pb_2Sb_2Te_5$.

PACS numbers:

* jhsong@pluto.phys.northwestern.edu

Topological insulators, distinguished from normal band insulators by a nontrivial Z_2 topological number and topologically protected surface states, have attracted great attention due to their significance both for applications and for fundamental research on a new quantum state of matter [1, 2]. Since the suggestion of a quantum spin Hall effect in a honeycomb lattice [3, 4], which is a time-reversal pair of Haldane models [5] and induced by spin-orbit interactions, several topological insulator materials were predicted and observed [6–12]. Efforts to find new topological insulators are still being made [13, 14]. A large spin-orbit coupling (SOC) strength is essential to realizing non-trivial topological band structures.

To classify the Z_2 topological number, we adopted the method proposed in ref. [15], which studied the topological phase transition by making a variation of external parameters such as the SOC strength or lattice constants. In our work, we varied the SOC strength ($\lambda_{\rm SO}$) from 0 to the real values of the systems (λ_0), and investigated whether the topological phase transition occurs. In three-dimensional (3D) topological insulator materials, a band crossing between conduction and valence bands should occur during this process: the 3D Dirac cone appears at the transition point between the band insulator (BI) and topological insulator (TI).

There are several advantages of this method. First, it is intuitive and only needs a direct observation of the Dirac cone at the transition point. Second, it does not require a heavy computational cost because of the simple unit-cell calculations. The surface calculations to see the topologically protected surface state are also one of alternative ways to determine the topological phase. The degrees of complexity of such calculations are, however, grater than the method we employed here. Third, this method can be applied to every system regardless of the existence of inversion symmetry. Lastly, the critical SOC value at which the band crossing occurs shows how far the system is located from the phase boundary of BI and TI.

By using this method, we found that the series of Pb-based chalcogenides, $Pb_nBi_2Se_{n+3}$ and $Pb_nSb_2Te_{n+3}$, are possible new candidates for TI materials and the topological phases are changed from TI to BI with increasing n. Among the above series, we focus on the material near the phase boundary between BI and TI due to the possibility of tuning the topological phase by changing external parameters.

To investigate the electronic structures and topological phases, first-principles calculations were performed using the full-potential linearized augmented plane wave method[16] with the gradient-corrected Perdew, Burke, and Ernzerhof form of the exchange-correlation functional [17]. The core states and the valence states were treated fully relativistically and scalar relativistically, re-

spectively. The calculations were carried out with the experimental lattice parameters for bulk $PbBi_2Se_4$, $PbSb_2Te_4$ and $Pb_2Bi_2Se_5$, and with the fully optimized geometry for the others, because crystal structures of $n = 1$ compounds and $Pb_2Bi_2Se_5$ were reported experimentally [18–20] and those of other n's are designed here theoretically.

$PbBi_2Se_4$ and $PbSb_2Te_4$ have the rhombohedral crystal structure, and a layered structure stacked along the c-axis of the hexagonal lattice, consisting of seven atoms in one septuple layer. The Pb atom is sandwiched by Se-Bi-Se or Te-Sb-Te layers and located at the inversion center, shown in Fig.1(a). There are van der Waals interactions between two septuple layers, and this provides a natural surface geometry which is appropriate for observing a topologically protected surface state.

Upon increasing the SOC strength ratio, $\lambda_{\rm SO}/\lambda_0$, from 0 to 1, both materials show the phase transition from BI to TI; in other words, there are band crossings during the process, cf., Fig1.(b)-(g). Critical values of the ratio are 0.46 for $PbBi_2Se_4$ and 0.62 for $PbSb_2Te_4$, and the electronic band structures at each critical point are shown in Fig.1(c) and Fig.1(f). 3D Dirac cones are seen at the Z point, one of the time-reversal invariant momentum points where -**k** is equivalent to **k**; they are doubly degenerate due to spatial inversion and time reversal symmetry.

Without the spin-orbit interaction, the system should have a trivial Z_2 topological number ($\nu = 0$), the so called BI. The presence of band crossings between conduction and valence bands during increasing SOC represents the change of its Z_2 topological number from trivial ($\nu = 0$) to non-trivial ($\nu = 1$) insulators. If the topological phase transition occurs before the SOC strength reaches λ_0, the system is classified as TI. In these inversion symmetric systems, band crossing is equivalent to band inversion where conduction and valence bands exchange their parities at the crossing point.

From our calculations, the bulk gaps of $PbBi_2Se_4$ and $PbSb_2Te_4$ are 0.28eV and 0.13eV, respectively. The gap size of $PbBi_2Se_4$ is comparable to that of Bi_2Se_3 [11, 12]. The gap values from the calculations without SOC are 0.24eV (Fig.1(b)) and 0.26eV (Fig.1(e)), which reflects purely hybridization effects. After increasing the SOC strength, gaps shrink to zero and then increase again, which shows the competition between hybridization and SOC strength in the topological phase transition. A non-trivial topological phase is a result of the predominance of SOC over the hybridization strength. Compared to other TI chalcogenides, the large band gap in $PbBi_2Se_4$ originates from weak hybridization and large SOC strength.

To estimate the gap size of $PbBi_2Se_4$ more precisely, we performed non-local screened-

exchange LDA (sX-LDA) calculations [21, 22] which overcome the well-known weakness of gap underestimation in the LDA scheme and reproduces the experimental gap values in many semiconducting materials. Significantly, the sX-LDA result yields a gap of 0.40eV in $PbBi_2Se_4$, which confirms that $PbBi_2Se_4$ is one of the largest gap TI, leading to the fact that $PbBi_2Se_4$ may be the best for high temperature applications among the known TI materials.

One advantage of the method, used in this work to verify the topological phase, is that it describes the exact distance from the phase boundary of BI and TI in terms of the SOC strength. For instance, the larger critical SOC strength of $PbSb_2Te_4$ than that of $PbBi_2Se_4$ means that the former is closer to the phase boundary than the latter.

In addition to $PbBi_2Se_4$ and $PbSb_2Te_4$, we suggest the series of $Pb_nBi_2Se_{n+3}$ and $Pb_nSb_2Te_{n+3}$ structures where n is an integer larger than 1 and show that a phase transition from TI to BI occurs as n increases. The crystal structure of $Pb_nBi_2Se_{n+3}$/ $Pb_nSb_2Te_{n+3}$ is composed of $(PbSe)_n$/$(PbTe)_n$ core with Se-Bi-(Se)/Te-Sb-(Te) sandwich layers. As shown in Fig.2(a), the critical SOC ratio (λ^c_{SO}/λ_0) exceeds 1 for $n \geq 3$ for both series of materials, which means that there is a phase boundary between $n = 2$ (TI) and $n = 3$ (BI). The gap sizes decrease up to $n = 2$ and increase again in going beyond the phase boundary. (cf. Fig.2(b)) On the other hand, the calculated gap values without SOC rise monotonically with n; this shows that as n increases, the hybridization strength exceeds SOC, resulting in the topological phase transition.

In Fig.2(c) and (d), electronic band structures from the slab geometry of the $n = 1$ and $n = 3$ composition of $Pb_nBi_2Se_{n+3}$, which consist of 6 septuple and 4 hendecuple layers with 78.4Å and 85.3Å respectively, are shown. Consistent with the critical SOC ratio in Fig.2(a), $PbBi_2Se_4$ has a topologically protected surface state, whereas there is no such state connecting the valence and conduction bands in the $Pb_3Bi_2Se_6$ slab. This is further evidence of the change in Z_2 topological number from 1 to 0 as n increases. The 2D surface state Dirac cone in the $PbBi_2Se_4$ slab is robust under the presence of non-magnetic perturbations. Again, the 0.35eV gap originating from bulk states is useful for high temperature spintronics applications. In other words, a single isolated surface state Dirac cone is seen in the energy range from -0.03eV below the Fermi level to 0.32eV above. In the case of the $Pb_3Bi_2Se_6$ slab, due to the weak van der Waals type interlayer interactions, no distinct surface state appears from the bulk BI states.

Among the Pb-based chalcogenides series, $Pb_2Sb_2Te_5$ whose critical SOC ratio is 0.96, is located quite close to the phase boundary, that its Z_2 topological number may be easily tuned by changing external parameters. The 26meV gap in the fully optimized geometry of $Pb_2Sb_2Te_5$

(Fig.3(a)) is closed by making a small change in lattice constants. As shown in Fig.3(b), $Pb_2Sb_2Te_5$ with a 0.5% reduction of the ab-lattice constants is positioned exactly at the borderline of TI and BI, whose electronic band structure shows a gapless 3D Dirac cone at the Γ point, realizing monopoles which generate an inverse-square type Berry curvature in the 3D Brillioun zone. A reduction of the ab-lattice constants makes the hybridization stronger, resulting in equilibration with the SOC strength. The band structure near the Dirac point shows anisotropic dispersions between in-plane and out-of-plane directions, described by a massless Dirac Hamiltonian

$$H = v_\perp \vec{\sigma}_\perp \cdot \vec{k}_\perp + v_\parallel \vec{\sigma}_\parallel \cdot \vec{k}_\parallel \tag{1}$$

where $\vec{\sigma}$ are Pauli matrices, $\vec{k}_\perp$ is a momentum vector along the c-axis and $\vec{k}_\parallel$ is on the ab-plane. Nearly circular cross-section on the (k_x-k_y) plane and an ellipsoidal cross-sections on the (k_z-k_x) plane are depicted in Fig.3(c) and (d), where the electronic band dispersion and the iso-energy contours of the 3D Dirac cone are shown.

The substitution of Te by Se might be useful to control the topological phase of this material in terms of varying both the SOC strength and lattice parameters. Considering the smaller ionic radius and SOC strength of Se than those of Te, the Se substitution can play a role in reducing not only lattice constants but also the SOC strength which can both accelerate the phase transition from TI to BI. Hence, $Pb_2Sb_2(Te_{1-x}Se_x)_5$ might be appropriate for studying the topological phase transition and the 3D Dirac cone.

In this work, we predicted new TI materials of Pb-based chalcogenides by investigating the change of the Z_2 topological number during variation of the SOC strength. With increasing n in the $Pb_nBi_2Se_{n+3}$ and $Pb_nSb_2Te_{n+3}$ series, the TI to BI transition occurs between $n = 2$ and 3. Among these compounds, $Pb_2Sb_2Te_5$ has a critical ratio of SOC strength close to 1, which means closeness to the phase boundary. Both topological phases and the gap at the 3D Dirac cone are tunable by changing lattice constants or the SOC strength. Also, it will be interesting to investigate the physical properties of the bulk 3D Dirac cone manifested at the critical point. As an extension of the present work, the $Pb_n(Bi/Sb)_{2m}(Se/Te)_{n+3m}$ series, which are pseudo-binary $[Pb(Se/Te)]_n[(Bi/Sb)_2(Se/Te)_3]_m$ systems and combinations of $Pb_n(Bi/Sb)_2(Se/Te)_{n+3}$ and $[(Bi/Sb)_2(Se/Te)_3]_m$ layered structures, are potential candidates for new TI materials which might show various bulk band gaps and topological phase transitions. The method used in our work can be the most appropriate tool to determine the Z_2 topological number of the systems without inversion symmetry, which show pair creation and annihilation of monopole and anti-monopoles

at the topological phase transition region [15].

ACKNOWLEDGMENTS

Support from the U.S. DOE under Grant No.DE-FG02-88ER45372 is gratefully acknowledged.

---

[1] M. Z. Hasan and C. L. Kane, http://www.arXiv.org/abs/1002.3895 (2010).

[2] X.-L. Qi and S.-C. Zhang, *Physics Today* **63**, 33 (2010).

[3] C. L. Kane and E. J. Mele, *Phys. Rev. Lett.* **95**, 226801 (2005).

[4] C. L. Kane and E. J. Mele, *Phys. Rev. Lett.* **95**, 146802 (2005).

[5] F. D. M. Haldane, *Phys. Rev. Lett.* **61**, 2015 (1988).

[6] B. A. Bernevig, T. L. Hughes, and S.-C. Zhang, *Science* **314**, 1757 (2006).

[7] M. Konig, S. Wiedmann, C. Brune, A. Roth, H. Buhmann, L. W. Molenkamp, X.-L. Qi, and S.-C. Zhang, *Science* **318**, 766 (2007).

[8] L. Fu, C. L. Kane, and E. J. Mele, *Phys. Rev. Lett.* **98**, 106803 (2007).

[9] D. Hsieh, D. Qian, L. Wray, Y. Xia, Y. S. Hor, R. J. Cava, and M. Z. Hasan, *Nature* **452**, 970 (2008).

[10] P. Roushan, J. Seo, C. V. Parker, Y. S. Hor, D. Hsieh, D. Qian, A. Richardella, M. Z. Hasan, R. J. Cava, and A. Yazdani, *Nature* **460**, 1106 (2009).

[11] Y. Xia, D. Qian, D. Hsieh, L. Wray, A. Pal, H. Lin, A. Bansil, D. Grauer, Y. S. Hor, R. J. Cava, and M. Z. Hasan, *Nat. Phys.* **5**, 398 (2009).

[12] H. Zhang, C.-X. Liu, X.-L. Qi, X. Dai, Z. Fang, and S.-C. Zhang, *Nat. Phys.* **5**, 438 (2009).

[13] S. Chadov, X. Qi, J. Kubler, G. H. Fecher, C. Felser, and S. C. Zhang, *Nat. Mater.* **9**, 541 (2010).

[14] H. Lin, L. A. Wray, Y. Xia, S. Xu, S. Jia, R. J. Cava, A. Bansil, and M. Z. Hasan, *Nat. Mater.* **9**, 546 (2010).

[15] S. Murakami and S.-i. Kuga, *Phys. Rev. B* **78**, 165313 (2008).

[16] E. Wimmer, H. Krakauer, M. Weinert, and A. J. Freeman, *Phys. Rev. B* **24**, 864 (1981).

[17] J. P. Perdew, K. Burke, and M. Ernzerhof, *Phys. Rev. Lett.* **77**, 3865 (1996).

[18] K. A. Agaev and S. A. Semiletov, *Kristallografiya* **13**, 258 (1968).

[19] L. E. Shelimova, O. G. Karpinskii, T. E. Svechnikova, E. S. Avilov, M. A. Kretova, and V. S. Zemskov, *Inorg. Mater.* **40**, 1264 (2004).

[20] K. A. Agaev, A. G. Talybov, and S. A. Semiletov, *Kristallografiya* **11**, 736 (1966).

[21] D. M. Bylander and L. Kleinman, *Phys. Rev. B* **41**, 7868 (1990).

[22] R. Asahi, W. Mannstadt, and A. J. Freeman, *Phys. Rev. B* **59**, 7486 (1999).

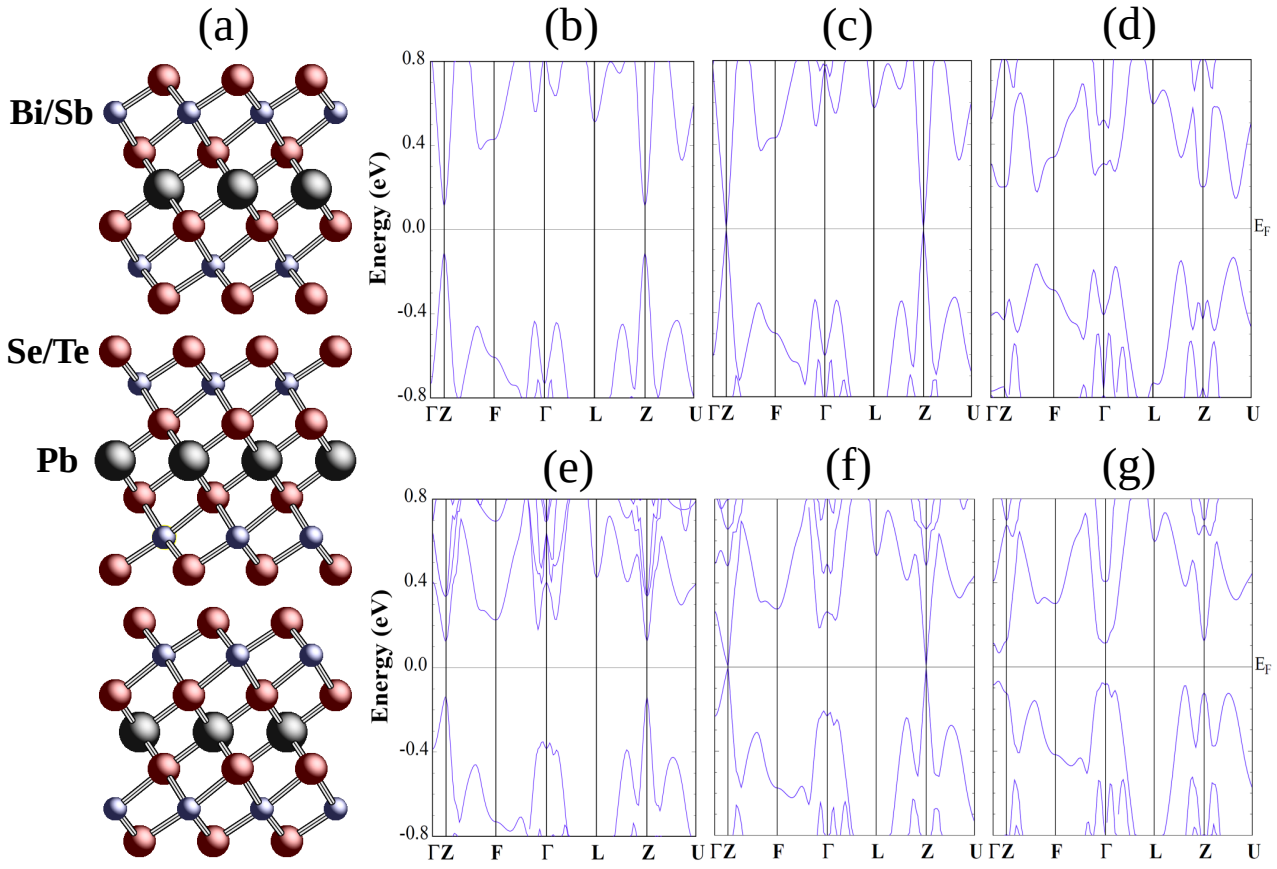

FIG. 1. (a) Crystal structures of $PbBi_2Se_4$/$PbSb_2Te_4$. Electronic band structures of (b)-(d) $PbBi_2Se_4$ and (e)-(f) $PbSb_2Te_4$. Calculations (b),(e) without spin-orbit interactions ($\lambda_{\rm SO} = 0$), (d),(g) with real SOC strength ($\lambda_{\rm SO} = \lambda_0$), and (c),(f) with critical SOC strength ($\lambda_{\rm SO} = \lambda^{\rm c}_{\rm SO}$).

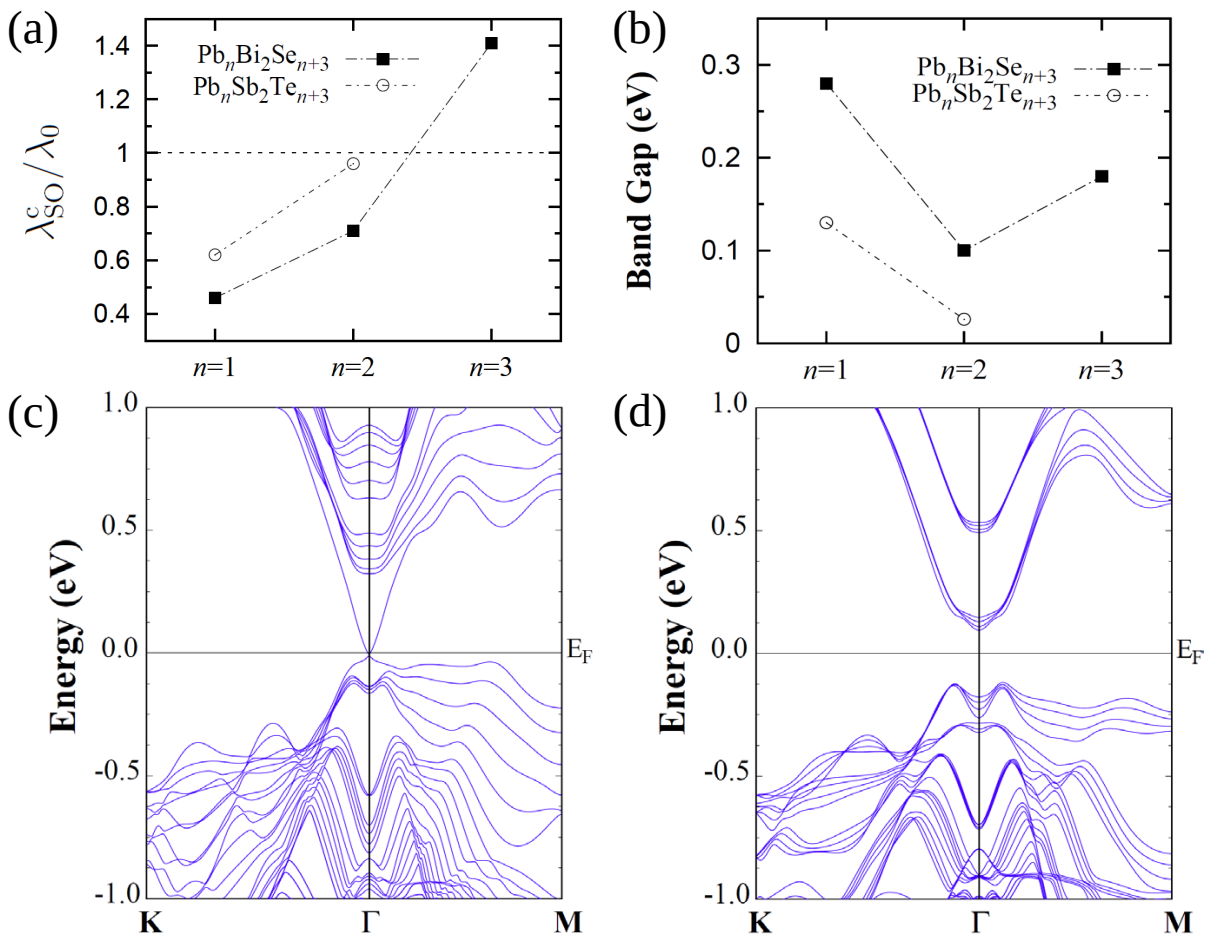

FIG. 2. (a) Critical SOC ratio and (b) bulk band gap with respect to n for the $Pb_nBi_2Se_{n+3}$ and $Pb_nSb_2Te_{n+3}$ series. Band structures of slab geometry of (c) 6 septuple layers of $PbBi_2Se_4$ and (d) 4 hendecuple layers of $Pb_3Bi_2Se_6$, which represent TI and BI, respectively.

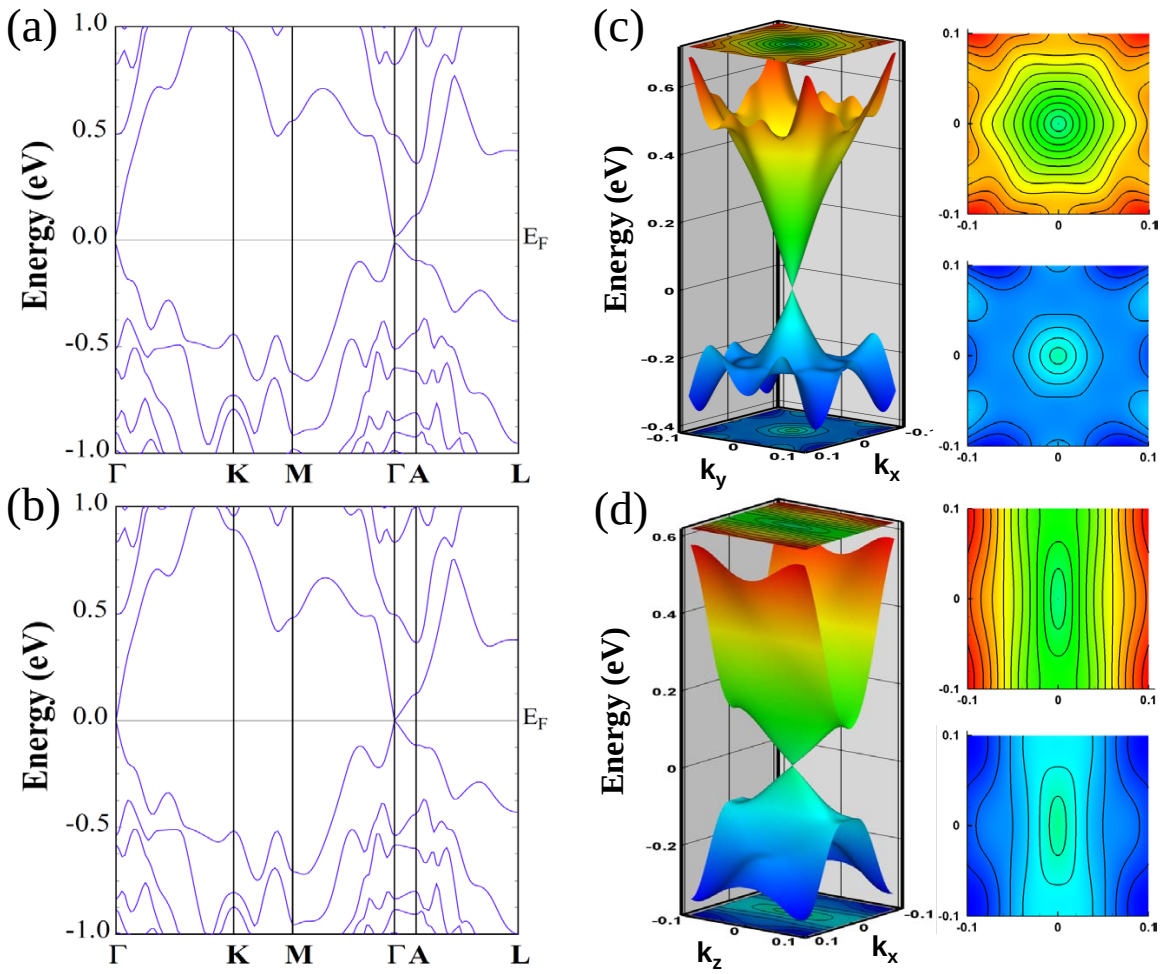

FIG. 3. Band structures of $Pb_2Sb_2Te_5$ with (a) fully optimized crystal structure and (b) 0.5% reduction of ab-lattice constants. Three-dimensional plot of Dirac cone in (b) and its contours are shown in (c) and (d). Anisotropic Dirac cone dispersions on (c) k_x-k_y and (d) k_z-k_x plane.